Sensors and Materials, Vol. 35, No. 2 (2023) 623–641
MYU Tokyo

S & M 3199

Is the Beijing–Tianjin–Hebei Region Experiencing More Frequent Wintertime Temperature Extremes?

Xi-ya Zhang,[1] Hai-bo Hu,[1] Yan-na Wang,[2]
Hong-liang Yan,[2] Yong-xue Wu,[3] and Ling-ling Shen[4*]

[1]Institute of Urban Meteorology, China Meteorological Administration,
No. 55 Beiwaxili, Haidian District, Beijing 100089, China
[2]Yanqing District Meteorological Bureau, Beijing Meteorological Administration,
No. 12 Hunan West Road, Yanqing District, Beijing 102199, China
[3]Huairou District Meteorological Bureau, Beijing Meteorological Administration,
No. 433 Liugechang Village, Huairou District, Beijing 101499, China
[4]Beijing Meteorological Data Center,
No. 10 Zhengfusi Middle Street, Haidian District, Beijing 100089, and China

(Received October 30, 2022; accepted January 19, 2023; online published February 13, 2023)

Keywords: copula function, return period, hazard risk, extreme temperature events

Extreme temperature events (ETEs) have occurred more frequently in recent winters in China. A comprehensive understanding regarding the probability of ETEs is important for the management and mitigation of the effects of such natural hazards. Using the temperature data from the air temperature sensor in the louver box and copulas from the technology of multivariate data analysis, in this study, we investigated the characteristics of ETEs and their implications for the Beijing–Tianjin–Hebei (BTH) region by analyzing the changing trends and probabilistic characteristics of eight indexes, including the frequency, duration, and intensity of ETE variables. Results showed that the study area has generally become warmer (regional averaged daily minimum temperature increased by 0.8 °C per decade) and has experienced more extreme cold events (ECEs) over the past 40 years. The probability of ECEs with more extreme cold days, longer duration, and lower temperatures has increased since 1999. Although the high risk of extreme warm events (EWEs) was calculated for the central BTH region, the most significant increase in risk of EWEs occurred in the colder northern BTH region. Furthermore, it cannot be ignored that the risk of concurrent ECEs and EWEs in most of the BTH region is high, and the probability of their co-occurrence is increasing. These probabilistic properties can provide important information for climate change, disaster risk assessments, and city geospatial governance.

1. Introduction

Within the context of global warming, the amplification of the Arctic, where the warming is greater than that of low latitude regions, increases the likelihood of the types of weather patterns

*Corresponding author: e-mail: shenlingling1988@qq.com
https://doi.org/10.18494/SAM4210

ISSN 0914-4935
https://myukk.org/

that lead to mid-latitude cold extremes.[1–3] Climate change will not only lead to abnormally high winter temperatures, but also highlight variation in the intensity and influence of extreme cold temperatures in wintertime. The occurrence of extreme temperature events (ETEs) in wintertime in China is becoming more likely.[4,5] Moreover, China is generally more vulnerable to ETEs than other countries owing to its high level of exposure.[6]

The trends or patterns of ETEs at regional and global scales have received increasing attention in recent decades.[7–10] Although many earlier studies have considered the variation of ETEs in China,[4,7,9] most focused on the changing patterns of several climate extreme indexes.[8,11,12] Following a study on the Loess Plateau (China), Sun *et al.* reported that the occurrence of cold extremes, including cold days and cold nights, decreased but that of extreme warm events (EWEs) increased.[8] You *et al.* reported that the Arctic Oscillation index can explain more than 50% of the change in winter temperature extremes in China.[11] Deng *et al.* documented an upward trend in the winter mean minimum temperature in the arid region of Northwest China over the past 50 years.[12] The mechanism underlying ETE variation is also a topic attracting wide interest.[1,11,13] Brown *et al.* reported that the positive phase of the North Atlantic Oscillation can cause EWEs for most of northern Eurasia and extreme cold events (ECEs) for southern Eurasia in winter.[13]

Clarification of the probabilistic behavior and assessment of the risk of ETEs remain to be fully documented. A number of recent observational and modeling studies revealed that rapid Arctic warming and associated sea ice loss might be increasing the risk of cold extremes.[2,10] However, fundamental aspects of some of the aforementioned studies have been questioned, and the future climate-induced risks of ETEs remain unclear.[1,3] Identifying the probability and/or risk of ETEs is very important for the management and mitigation of the effects of such natural hazards.[5] An ETE is a multivariate phenomenon characterized by multiple variables such as temperature threshold, duration, frequency, and interval. Knowledge of the joint probabilistic characteristics of ECEs would provide more helpful information that could support in-depth understanding of the response of climatic mechanisms to climate change.

The 2022 Winter Olympic Games were held in the Beijing–Tianjin–Hebei (BTH) region of China, and either ECEs or EWEs in wintertime could have had a substantial influence on this event. Therefore, it was imperative to perform comprehensive evaluation of the risk and probability of ETEs in the BTH region in wintertime. The objectives of this study are as follows: (1) study the change characteristics and probabilistic characteristics of ETEs, (2) analyze the joint probabilistic characteristics and trends of bivariate ETEs, and (3) evaluate the risk of ETEs in the BTH region in wintertime to provide useful information pertaining both to climate change in general and to the 2022 Winter Olympic Games in particular. The remainder of this paper is organized as follows. Section 2 describes the dataset and method used. The results of the bivariate ETEs and risk analysis for ETEs are provided in Sect. 3. Section 4 discusses the probabilistic characteristics of ETEs. Finally, the conclusions are presented in Sect. 5.

2. Data and methodology

2.1 Study area and data used

The study area of the BTH region is located in northern China (Fig. 1), including Beijing, Tianjin, and eight neighboring cities in China's Hebei Province. The BTH region is located in eastern Asia and has a continental monsoon climate featuring dry and cold winters. The minimum absolute temperature may be lower than −30 °C in bitterly cold winters, whereas the maximum absolute temperature may be higher than 20 °C in warm winters.

Observational daily minimum temperature and daily maximum temperature data from 176 meteorological stations in the BTH region were used in this study (Fig. 1). The air temperature data used in this paper were all from the air temperature sensor in the louver box of the national surface meteorological observation station and provided by the Chinese Meteorological Administration, which performs prerelease data quality checks. Considering the availability and reliability of the data used, we focused on 40 boreal winter seasons (November–March) in the period 1978/11–2018/03. Although the missing data represented < 0.01% of the total data, there were some missing values in the daily temperature dataset. These missing values were filled using the average values of adjacent days. This gap-filling method has no effect on the long-term temporal trends. The meteorological stations are sparse in mountainous areas, but dense on plains, especially in urban areas.(5)

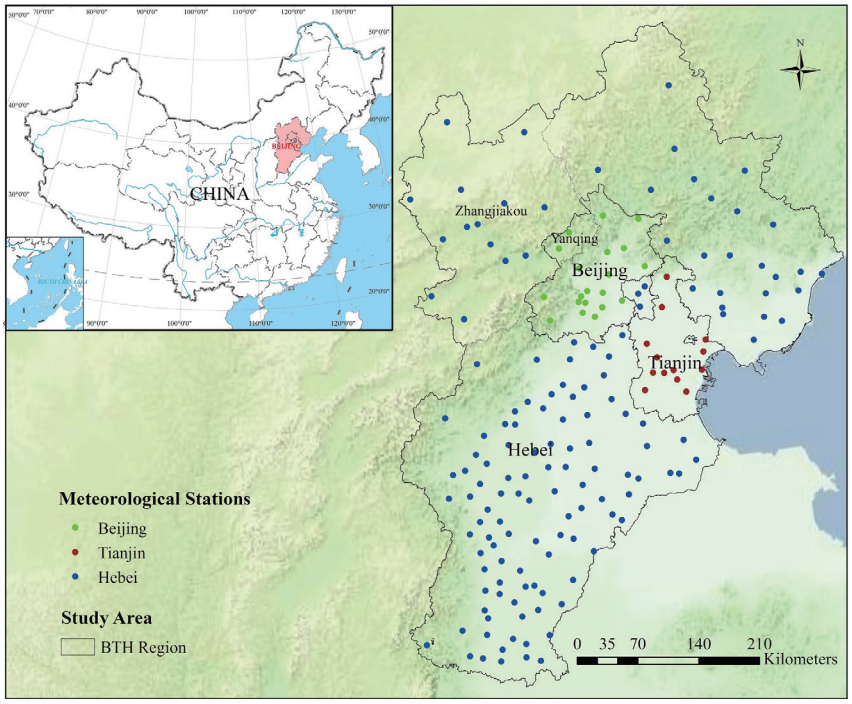

Fig. 1. (Color online) Map showing the BTH region and the locations of the meteorological stations used in the study.

2.2 Definition of wintertime temperature extremes

In this study, an extreme cold day (ECD) was defined as a day with a daily minimum temperature below the 5th percentile of the local distribution of daily minimum temperature during November–March. An extreme warm day (EWD) in wintertime was defined as a day with a daily maximum temperature above the 5th percentile of the local distribution of daily maximum temperature during November–March. These definitions established ECD and EWD thresholds for each meteorological station. The distribution of those threshold temperatures is illustrated in Fig. 2. The lowest ECD thresholds mostly correspond to the northern BTH region, and the ECD threshold at Kangbao Station in Hebei Province is as low as −29 °C. The highest EWD thresholds are concentrated in the southern BTH region, and the EWD threshold at Shexian Station in Heibei Province is as high as 20 °C.

In this study, ECEs were identified from consecutive occurrences of ECDs. If the daily minimum temperature persisted below the ECD threshold for more than one day, we regarded the persistent ECDs as an ECE. Similarly, EWEs were defined as persistent EWDs for which the daily maximum temperature met or exceeded the EWD thresholds for more than one day. For the purposes of this study, ECEs were characterized by four cold indexes: the number of ECDs (ECDN), mean minimum temperature of ECDs (ECDT), ECE duration (ECED), and ECE intensity (ECEI). Duration refers to the number of days an event lasted, whereas intensity reflects the mean temperature over the entire event. Similarly, EWEs were characterized by four warm indexes that were defined in the same manner as the ECE indexes. The definitions and units of these indexes are summarized in Table 1.

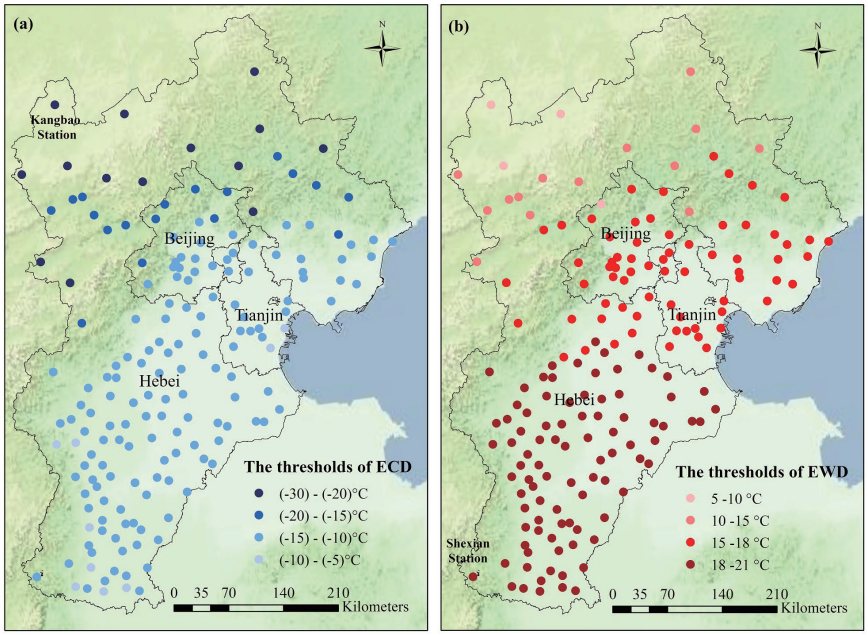

Fig. 2. (Color online) Distribution of extreme temperature thresholds in the BTH region during boreal winter: (a) ECD thresholds and (b) EWD thresholds.

Table 1
ETE indexes defined in this study.

ETEs	Abbreviations	Units	Definitions
ECE	ECDN	days	Number of ECDs in a year
	ECDT	℃	Average minimum temperature of ECDs in a year
	ECED	days	Maximum duration of ECEs in a year
	ECEI	℃	Intensity of ECE with maximum duration in a year
EWE	EWDN	days	Number of EWDs in a year
	EWDT	℃	Average maximum temperature of EWDs in a year
	EWED	days	Maximum duration of EWEs in a year
	EWEI	℃	Intensity of EWE with maximum duration in a year

2.3 Analysis of wintertime temperature extremes and return levels

First, the Mann–Kendall trend test was used to detect the trend of the selected index in the analysis of the time series trend of ECEs and EWEs. We used $\alpha = 0.05$ to determine the statistical significance of a trend. The trends were also calculated for the regional scale using the linear least squares method. Next, to analyze the distributions of the ETE indexes, we considered six distributions: normal, gamma, generalized extreme value, extreme value, three-parameter lognormal, and Weibull distributions. Maximum likelihood estimation was used to estimate the parameters of these distribution functions. The goodness-of-fit of the probability function was assessed using the Kolmogorov–Smirnov test to select the appropriate distribution for each ETE index. The 5-year return levels for the indexes over the entire time series were calculated using the selected distribution. To analyze the trends of the 5-year return levels for these two types of ETE, data from 1978–2015 for each event were divided into two periods: 1978–1998 and 1999–2015. Thereafter, the 5-year return levels from the two periods were generated.

2.4 Copula selection and joint return periods

Copulas can provide flexible representations of multivariate distributions.[14–16] A copula function can fit each variable separately to a marginal distribution and then concatenate them together. The copula function has been widely used to analyze hydrometeorological extremes such as drought, rainfall, and floods.[17–19] Previous studies have shown that a copula function can provide satisfactory multivariate joint distributions and associated event frequency analyses.[5]

In this study, we selected Archimedean copulas, including the Clayton, Gumbel–Hougaard, and Frank copulas to analyze the joint probability of ECEs. These copulas were also used in our previous study of ECEs where descriptions of the copula distributions can be found.[5] The maximum likelihood method was used to estimate the parameters of the copula. Copula functions were evaluated using an empirical copula function.[20] The root mean square error (RMSE) was used to estimate the degree-of-fit between the empirical copula and the theoretical copula.[21] The RMSE can be expressed as follows:

$$RMSE = \sqrt{\frac{1}{n}\sum_{i=1}^{n}[C_p(i) - C_e(i)]^2}\ , \tag{1}$$

where n is the sample size, C_p denotes the computed values of the theoretical copula, and C_e denotes the observed values of the probability obtained from the empirical copula. The copula function with the lowest RMSE value was chosen.

Our previous results showed that calculating a return period using copula functions can serve as an accurate and convenient framework for risk assessment of extreme events.[5] In this study, two joint return periods were computed using the selected copula as follows:

$$T_{\{X>x,Y>y\}} = \frac{1}{P(X>x,Y>y)} = \frac{1}{1-F_x(x)-F_y(y)+C(F_x(x),F_y(y))}, \tag{2}$$

$$T_{\{X>x,Y<y\}} = \frac{1}{P(X>x,Y<y)} = \frac{1}{F_y(y)-C(F_x(x),F_y(y))}, \tag{3}$$

where $T_{\{X>x,\ Y>y\}}$ denotes a joint return period when both X and Y exceed the specific threshold; $T_{\{X>x,\ Y<y\}}$ is a joint return period when X exceeds the specific threshold while Y is less than the specific threshold; $P(X>x,\ Y>y)$ and $P(X>x,\ Y<y)$ denote the probability of the corresponding events; $F_x(x)$ and $F_y(y)$ are the marginal distribution functions for variables X and Y, respectively; and $C(F_x(x),\ F_y(y))$ represents the copula function that is the corresponding joint probability distribution. In this study, the threshold value used for each variable was its regional average of the 5-year return level, which can be expressed as follows:

$$\overline{R}_5 = \frac{\sum_{i=1}^{n} R_i}{n}, \tag{4}$$

where $\overline{R}_5$ is the regional average of the 5-year return level for one index, R_i is the 5-year return level of some index for station i, and n is the number of stations.

Several combinations were selected to analyze the risk of ETEs. The terms $T_{\{ECDN>\overline{ECDN_5},ECDT<\overline{ECDT_5}\}}$ and $T_{\{ECED>\overline{ECED_5},ECEI<\overline{ECEI_5}\}}$ were used to reflect the characteristics of ECEs, and $T_{\{ECED>\overline{ECED_5},ECEI<\overline{ECEI_5}\}}$ also represented ECEs with long duration and low temperatures that might have a considerable influence on human society. The terms $T_{\{EWDN>\overline{EWDN_5},EWDT>\overline{EWDT_5}\}}$ and $T_{\{EWED>\overline{EWED_5},EWEI>\overline{EWEI_5}\}}$ were used to investigate the characteristics of EWEs, and $T_{\{EWED>\overline{EWED_5},EWEI>\overline{EWEI_5}\}}$ was used to investigate the characteristics of the co-occurrence of extremely long warm periods and high temperatures. Additionally, the term $T_{\{ECDN>\overline{ECDN_5},EWDN>\overline{EWDN_5}\}}$ was constructed to analyze the characteristics of the ECEs and EWEs encountered within a year. Finally, the change trends of the joint return periods were also studied using the same method as above for the 5-year return levels.

2.5 Spatial–temporal clustering method

We investigated the spatial–temporal relationship and interaction between the two types of ETEs in wintertime by analyzing the spatial–temporal clustering characteristics of the two ETEs. Spatial–temporal clustering is a process that groups objects on the basis of their spatial and temporal similarities. It is one of the fundamental elements of data mining and is important for revealing the spatial–temporal pattern, process evolution, and mechanism of geographic elements through a comprehensive consideration of the spatial–temporal coupling factors.[22] Spatial–temporal clustering analysis has been applied widely in the fields of global climate change, public health security, earthquake monitoring, and crime hotspot analysis. However, few studies have applied spatial–temporal clustering to the analysis of extreme climate events or disaster risk assessment.

An ETE is a type of spatial–temporal information, and each event is usually associated with the location where it was recorded and the corresponding timestamp. In this study, the space–time scan statistic was used to analyze the temporal and spatial variation characteristics of ECEs and EWEs in the BTH region. The space–time scan statistic is determined by gradually scanning a window across time and space, where the scanning window is a cylinder with a circular (or elliptical or network-based) geographic base and a height that corresponds to time. The base represents distinct geographic circles with different sets of neighboring data locations within them, whereas the height reflects the time period of potential clusters. The cylindrical window is then moved in space and time such that each possible geographic location and size is visited for each possible time period. In the scanning process, the statistical test method is used to determine possible clusters of disaster events and to elucidate their spatial–temporal clustering characteristics. In this study, SatScan v9.5 software was used to perform spatial–temporal clustering analysis.[23,24] Identification of spatial high/low clusters was achieved using the space–time permutation model assumption.[24] The minimum temporal cluster size was 30% of the study period, and 999 Monte Carlo replications were performed. The null hypothesis of no significant clusters was rejected when the simulated p-value was ≤ 0.05.

3. Results

3.1 Variation of wintertime temperature extremes

In terms of ECDN, most stations exhibited decreasing trends, and 48% of the total number of stations showed significant decreasing trends. Only 14 out of 175 stations had increasing trends, and the increases were not significant ($p > 0.01$) [Fig. 3(a)]; these stations were located mainly in the western and northern mountainous areas of Beijing and the northern area of Hebei. It can be seen from Fig. 3(b) that 86% of the total number of stations indicated increasing tendencies in ECDT, and that the trends for 30% of these stations were significant ($p < 0.01$). Only two stations showed significant decreasing trends: Tanghekou Station in Beijing and Qinhuangdao Station in Hebei Province. A comparison of Fig. 3(a) and 3(b) reveals that the daily minimum temperature exhibited decreasing trends in areas

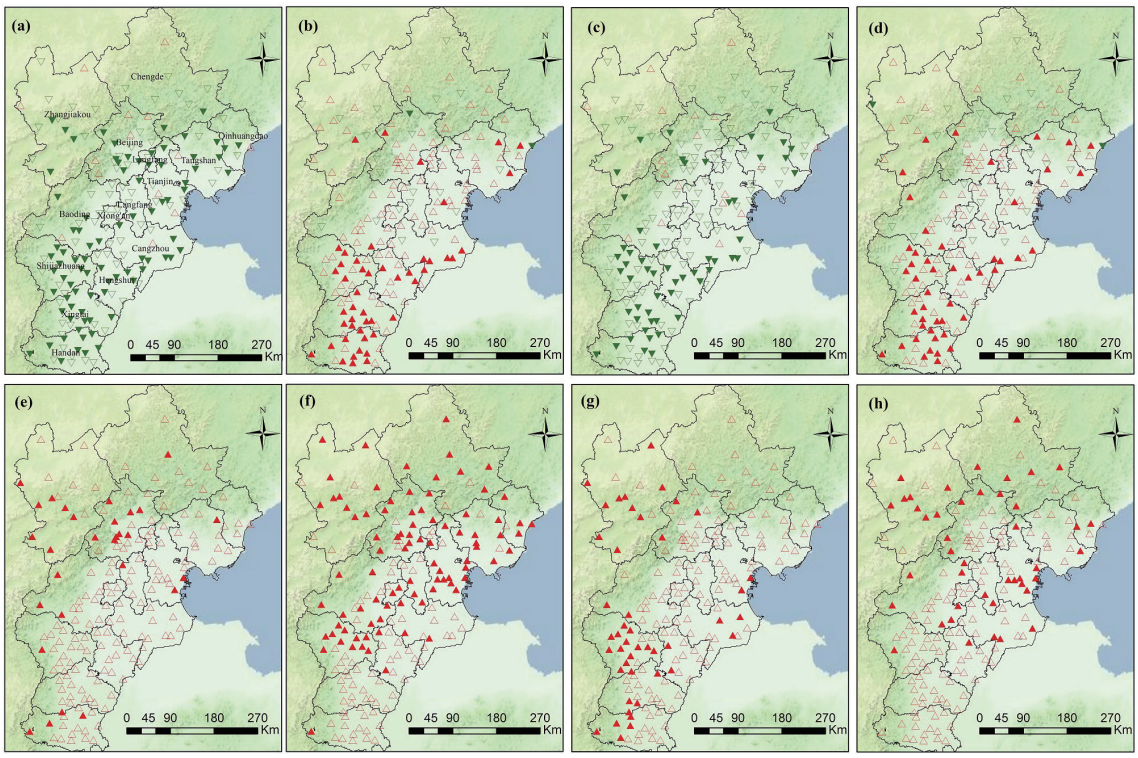

Fig. 3. (Color online) Spatial distributions of annual trends in (a) ECDN, (b) ECDT, (c) ECED, (d) ECEI, (e) EWDN, (f) EWDT, (g) EWED, and (h) EWEI. Filled red triangles denote significant increases, inverted filled green triangle denote significant decreases, inverted open green triangles denote no significant decrease, and open red triangles denote no significant increase.

where extreme cold days increased. For ECED, 90% of stations showed decreasing trends, and for most stations in southern Hebei, the decrease was significant [Fig. 3(c)]. The stations that showed increasing trends were located mainly in the northern parts of Beijing and Hebei Province. Most stations showed increasing trends in ECEI; however, those ECEs with increasing duration had an average minimum temperature decrease [Fig. 3(d)]. Overall, although most stations in the BTH region showed a decrease in ECEs, approximately 10% of stations had an increase in ECEs, and 16% of those sites experienced more severe ECEs with longer duration and lower temperature.

All stations indicated increasing tendencies in EWDN [Fig. 3(e)], and for 16% of the stations, the trend was significant ($p < 0.01$). The distribution of sites with a significant increase in EWDN was similar to that of sites with increasing ECDN. In terms of EWDT, more than 50% of stations showed a significant increasing trend. Some sites reflected the marked increase in temperature in urban areas, e.g., Shijiazhuang, Beijing, and Tianjin, whereas others reflected the more notable increase in daily maximum temperature in areas with colder winters, e.g., the mountainous areas in northern Beijing, and Zhangjiakou and Chengde in Hebei Province [Fig. 3(f)]. Overall, 25% of stations showed significant increasing trends in EWED, and these stations were located mainly in northwestern and

southeastern parts of Yunnan. The other stations exhibited increasing trends in the duration of EWEs, but the increases were not significant [Fig. 3(g)]. The changes in EWEI appear complex [Fig. 3(h)]. In urban areas, although the duration of EWEs increased significantly, the temperature increase of EWEs with long duration was not significant. At some mountain sites, the duration of EWEs increased significantly, and the temperature increase of long-lasting EWEs was also significant. Generally, EWEs had increasing trends in EWDN, daily maximum temperature, or duration and intensity of EWEs. It should be noted that some stations in northern Beijing, Zhangjiakou, and northern Chengde indicated increasing tendencies in EWEs and ECEs.

Overall, the BTH region has generally become warmer, as demonstrated by the lower frequency and duration of ECEs, higher frequency and duration of EWEs, and increasing values of minimum and maximum temperatures.

On the regional scale, the results in Fig. 4 show that the regional averaged ECDN decreased significantly over the previous several decades, whereas the decrease in ECED was insignificant ($p > 0.01$). The regional mean ECDN and ECED decreased by 2.2 and 0.5 d per decade, respectively. The regional averaged ECDT and ECEI increased, although the increases were not significant. The regional averaged daily minimum temperature increased by 0.8 °C per decade over the past 40 years, and the averaged temperature of ECEs with long-lasting duration increased by 0.88 °C per decade in boreal winter. The EWDN and the duration of EWEs increased significantly; the regional averaged EWDN and EWED increased by 1.2 and 0.68 d per decade, respectively. The change in the daily maximum temperature was insignificant in wintertime, and EWDT decreased slightly, which is different from the change in daily minimum temperature in ECEs.

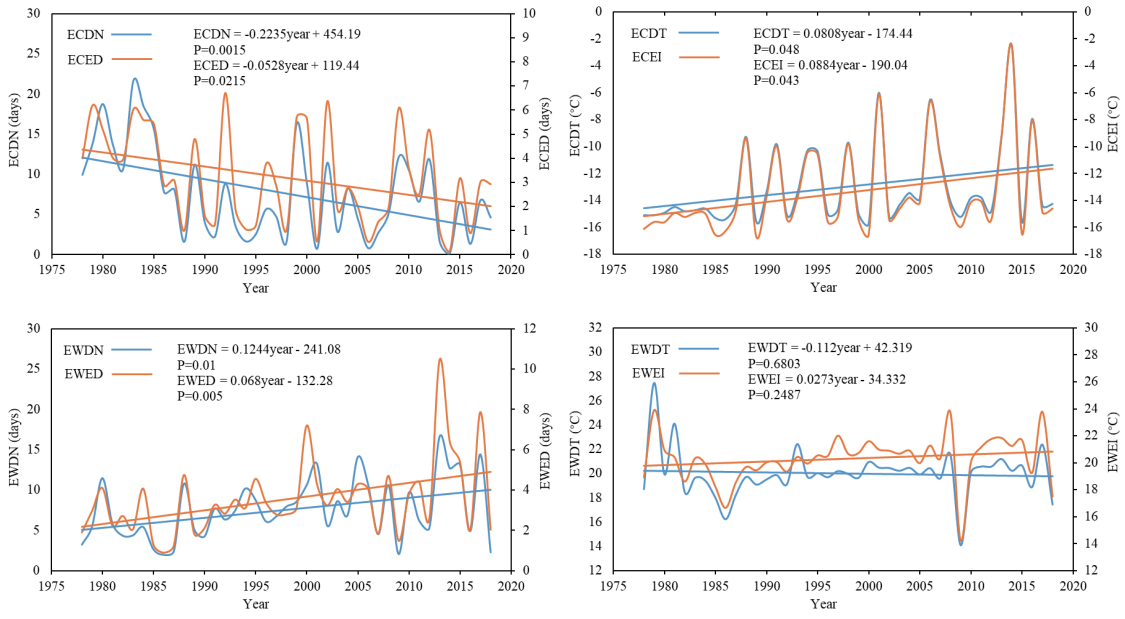

Fig. 4. (Color online) Dynamics of regional averaged ETE indexes in the BTH region.

3.2 Spatial distribution and changing trends of 5-year return levels

The 5-year return levels of the ETE indexes were calculated after the selection of the best distributions for each station. Here, the indexes of $ECDN_5$, $ECDT_5$, $ECED_5$, $ECEI_5$, $EWDN_5$, $EWDT_5$, $EWED_5$, and $EWEI_5$ refer to those 5-year return levels. The 5-year return levels generally represent the maximum magnitudes of the indexes at 80% occurrence probability.

The spatial distributions of the 5-year return levels are shown in Fig. 5. The $ECDN_5$ values were generally large in the middle of the BTH region, and the values for most stations were in the range of 10–15 d [Fig. 5(a)]. The spatial distribution of $ECDT_5$ varied greatly. The $ECDT_5$ values were generally low in the northern BTH region and exhibited an apparent upward trend from the north toward the south [Fig. 5 (b)]. Overall, 13 stations had $ECDT_5$ values lower than −20 °C, and 15 stations had values in the range of −20 to −15 °C. The spatial distributions for $ECED_5$, $ECEI_5$, and $ECDT_5$ were similar, with the three indexes exhibiting increasing trends from the north toward the south. The largest values of $ECED_5$, $ECEI_5$, and $ECDT_5$ were observed in the region of the cities of Tianjin and Shijiazhuang [Fig. 5 (b)–(d)]. The values of $EWDN_5$ were mainly around 10 d. For most stations, the value of $EWDT_5$ was >15 °C, but it was lower than 0 °C for a few stations in Yanqing District in Beijing [Fig. 5 (f)]. The $EWED_5$ values were mainly around 5 d, but for stations in northern Zhangjiakou, they were around 3 d. Most stations had $EWEI_5$ values above 15 °C, but a few stations in Zhangjiakou had values of around 10 °C.

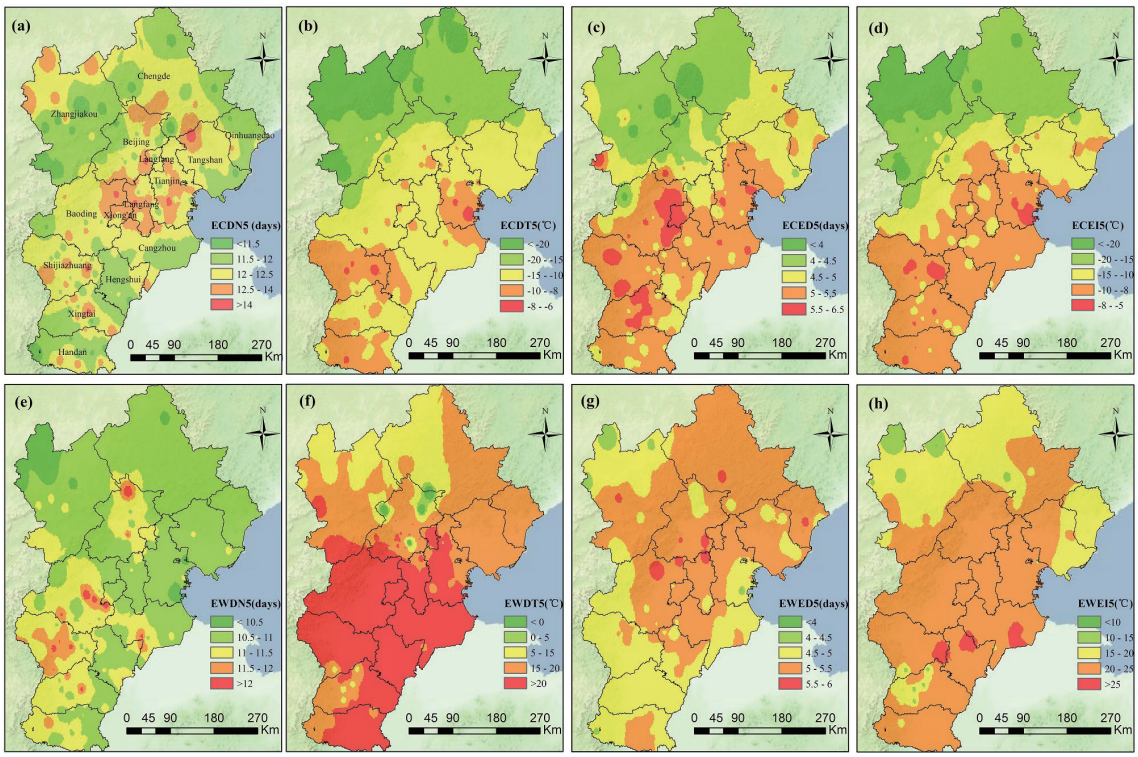

Fig. 5. (Color online) Spatial distributions of (a) $ECDN_5$, (b) $ECDT_5$, (c) $ECED_5$, (d) $ECEI_5$, (e) $EWDN_5$, (f) $EWDT_5$, (g) $EWED_5$, and (h) $EWEI_5$. All the ETE indexes plotted in this figure are for 5-year return periods.

To analyze the changes in the 5-year return levels for the ETE indexes, the 5-year return levels of the ETE indexes were calculated for two periods: 1978–1998 and 1999–2018. Figure 6 shows the changes in the 5-year return levels of the eight indexes during 1999–2018 relative to 1978–1998. Overall, the majority of stations experienced significant trends in the 5-year return levels. It can be seen from Fig. 6(a) that the $ECDN_5$ in northern Hebei Province generally increased, but that in most of the rest of the region showed a downward trend, especially in Shijiazhuang and surrounding areas. As for $ECDT_5$ [Fig. 6(b)], most stations had increasing trends, whereas some stations in northern Chengde and Zhangjiakou experienced downward trends. The range of changes in $ECED_5$ is very small, and the change trend is similar to that of $ECDN_5$ [Fig. 6(c)]. The distribution of $ECEI_5$ and $ECDT_5$ is somewhat different. For $ECEI_5$, some sites in the northwest of Baoding showed a downward trend, whereas some sites in Zhangjiakou showed an upward trend [Fig. 6(d)]. For $EWDN_5$ and $EWED_5$, increasing trends were observed throughout the BTH region [Figs. 6(e) and 6(g)]. Generally, $EWDN_5$ increased by approximately 5 d for most sites, and $EWED_5$ increased by approximately 3 d for most sites. Both $EWDT_5$ and $EWEI_5$ exhibited a tendency to increase across a large part of the study area, except in some areas of Xingtai, Chengde, and Zhangjiakou [Figs. 6(f) and 6(h)].

The regional averaged values of the 5-year return levels of the ETE indexes are presented in Table 2. In comparison with the values in 1978–1998, $ECDN_5$ and $ECED_5$ decreased by 4.13 and

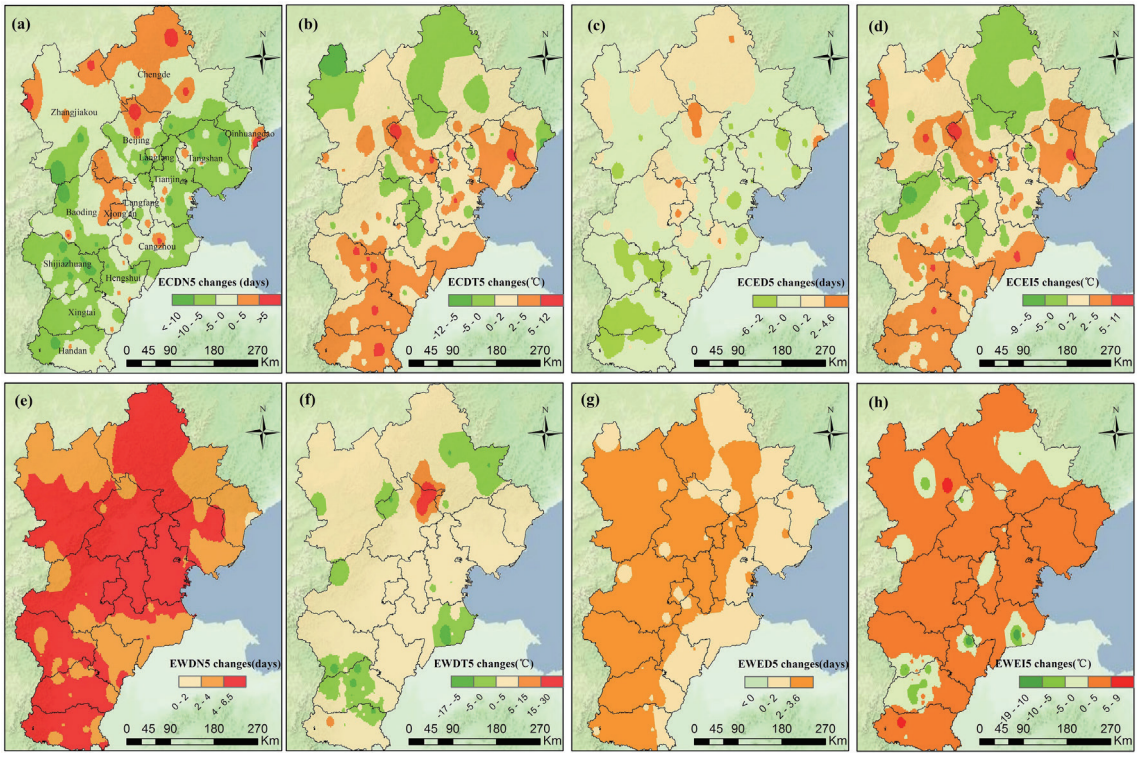

Fig. 6. (Color online) Spatial distributions of changing patterns of (a) $ECDN_5$, (b) $ECDT_5$, (c) $ECED_5$, (d) $ECEI_5$, (e) $EWDN_5$, (f) $EWDT_5$, (g) $EWED_5$, and (h) $EWEI_5$. Filled red triangles denote increases, inverted filled green triangles denote decreases.

Table 2
The 5-year return levels for the regional averaged indexes in the two periods studied: 1978–1998 and 1999–2018.

Index	1978–1998	1999–2019	Changes
$ECDN_5$ (days)	14.28	10.14	−4.13
$ECDT_5$ (°C)	−12.72	−11.11	1.61
$ECED_5$ (days)	5.41	4.53	−0.88
$ECEI_5$ (°C)	−12.38	−10.78	1.60
$EWDN_5$ (days)	8.74	13.07	4.34
$EWDT_5$ (°C)	20.14	21.08	0.94
$EWED_5$ (days)	3.94	6.10	2.16
$EWEI_5$ (°C)	21.40	22.12	0.72

0.88 d, whereas $EWDN_5$ and $EWED_5$ increased by 4.34 and 2.16 d, respectively. Both $ECDT_5$ and $ECEI_5$ increased by approximately 1.6 °C, whereas $EWDT_5$ and $EWEI_5$ increased by 0.94 and 0.72 °C, respectively. These results also show the impact of global warming on winter in the BTH region. Under the certain risk of 5-year return levels, the duration of the longest ECE in the BTH region during 1999–2018 decreased in comparison with that of the earlier period, and the average minimum temperature of the ECEs showed an upward trend. Both the duration of EWEs and the average maximum temperature have increased.

3.3 Copula selection for joint distribution of wintertime temperature extremes

The empirical and copula-based joint distributions of different pairs of indexes, shown in Fig. 7, indicate that the copula-based distribution does reflect the dependence structure of the ETE indexes.

As shown in Fig. 8(a), small $T_{\{ECDN>\overline{ECDN_5},ECDT<\overline{ECDT_5}\}}$ values were observed in most of the BTH region, i.e., generally <10 years. This observation implies a higher probability of concurrent long ECDN and low ECDT in most of the area. In other words, the risk of occurrence of ECDs within a year is higher in the BTH region. Figure 8(b) shows the probability distribution patterns of long ECED and low ECEI. The $T_{\{ECED>\overline{ECED_5},ECEI<\overline{ECEI_5}\}}$ values are generally <15 years in most of the area, implying higher risk of occurrence of ECEs. Relatively high values of $T_{\{ECED>\overline{ECED_5},ECEI<\overline{ECEI_5}\}}$ occurred mainly in the southernmost part of Hebei Province, with less risk of occurrence of ECEs within a year. Figure 8(c) illustrates the distribution of $T_{\{EWDN>\overline{EWDN_5},EWDT>\overline{EWDT_5}\}}$ values, reflecting the probability of concurrent long EWDN and low EWDT. This probability was small in northern parts of Hebei Province, but relatively high in the middle of the study area. Figure 8(d) shows the probability distribution patterns of long EWED and high EWEI. High $T_{\{EWED>\overline{EWED_5},EWEI>\overline{EWEI_5}\}}$ values were generally found in most of the BTH region, which means less risk of occurrence of long EWED and high EWEI. Relatively high risk of occurrence of EWE occurred only in the cities of Baoding, Langfang, and Hengshui in Hebei Province. The $T_{\{ECDN>\overline{ECDN_5},EWDN>\overline{EWDN_5}\}}$ values in most areas were <10 years, and relatively high values were noted mainly in the cities of Shijiangzhuang and Tianjin [Fig. 8(e)], indicating that the probability of concurrent ECDs and EWDs was lower in the cities of Shijiangzhuang and Tianjin, but relatively high in other areas.

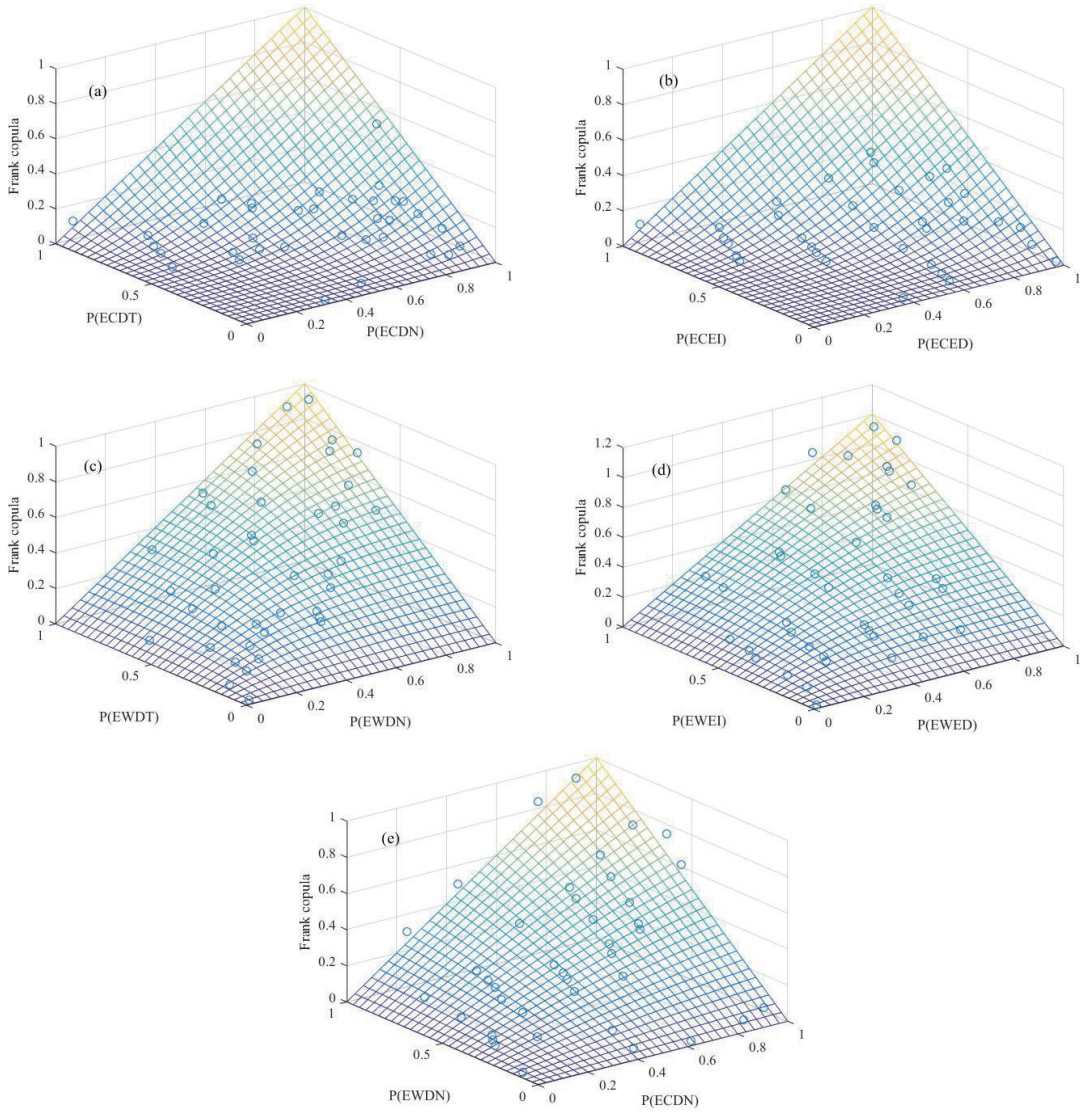

Fig. 7. (Color online) Empirical and copula-based distributions for different pairs of indexes: (a) ECDN and ECDT, (b) ECED and ECEI, (c) EWDN and EWDT, (d) EWED and EWEI, and (e) ECDN and EWDN at the Beijing station.

Overall, the results shown in Figs. 8(a) and 8(b) indicate that the probability of concurrent extreme cold and a long-lasting ECEs was larger in most of the BTH region. The results for the middle of the BTH region were relatively more complex. Parts of the middle region, such as Beijing, Baoding, and Langfang, were at greater risk of EWEs in wintertime [Figs. 8(c) and 8(d)], but large values of $T_{\{ECDN>\overline{ECDN_5},EWDN>\overline{EWDN_5}\}}$ and $T_{\{ECED>\overline{ECED_5},ECEI<\overline{ECEI_5}\}}$ in these cities also reflected that these areas are at high risk of ECEs [Figs. 8(a) and 8(b)]. Furthermore, the low $T_{\{ECDN>\overline{ECDN_5},EWDN>\overline{EWDN_5}\}}$ values suggest high risk of concurrent ECEs and EWEs [Fig. 8(e)].

The changes reflecting different joint return periods are illustrated in Fig. 9. The variation pattern of the joint return periods shows certain spatial heterogeneity. In most areas, the

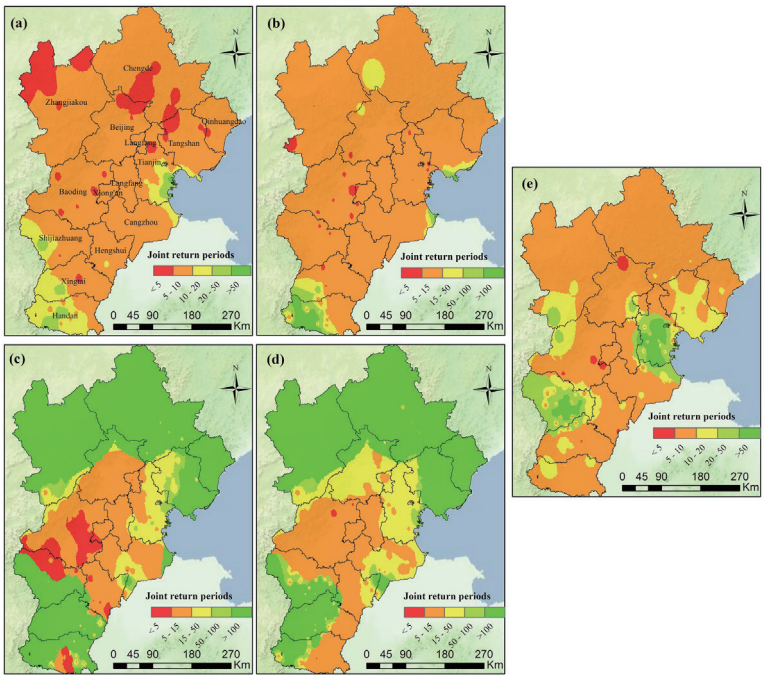

Fig. 8. (Color online) Distributions of joint return periods for different bivariate ETEs: (a) $T_{\{ECDN>\overline{ECDN_5},ECDT<\overline{ECDT_5}\}}$, (b) $T_{\{ECED>\overline{ECED_5},ECEI<\overline{ECEI_5}\}}$, (c) $T_{\{EWDN>\overline{EWDN_5},EWDT>\overline{EWDT_5}\}}$, (d) $T_{\{EWED>\overline{EWED_5},EWEI>\overline{EWEI_5}\}}$, and (e) $T_{\{ECDN>\overline{ECDN_5},EWDN>\overline{EWDN_5}\}}$.

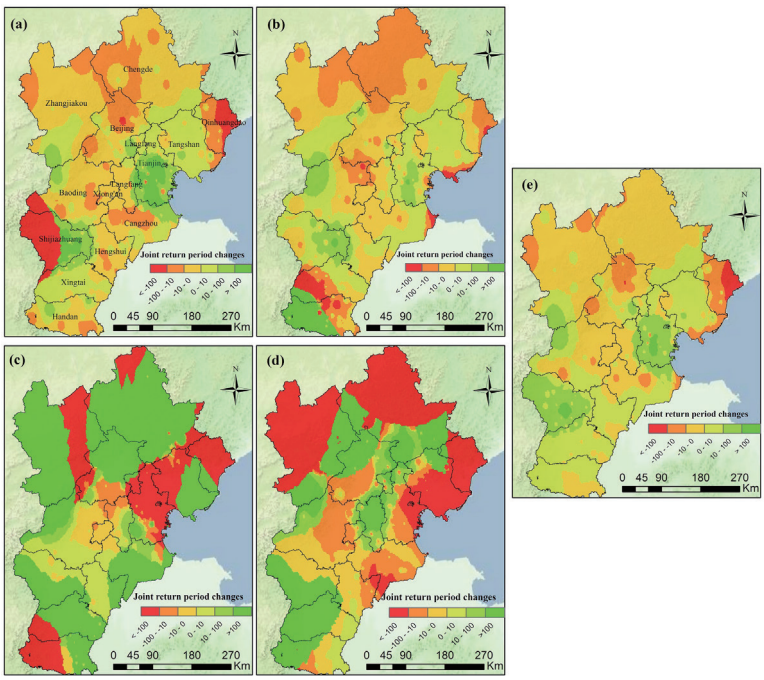

Fig. 9. (Color online) Spatial distributions of changing patterns for different joint return periods for different bivariate ETE indexes: (a) $T_{\{ECDN>\overline{ECDN_5},ECDT<\overline{ECDT_5}\}}$, (b) $T_{\{ECED>\overline{ECED_5},ECEI<\overline{ECEI_5}\}}$, (c) $T_{\{EWDN>\overline{EWDN_5},EWDT>\overline{EWDT_5}\}}$, (d) $T_{\{EWDN>\overline{EWDN_5},EWDT>\overline{EWDT_5}\}}$, and (e) $T_{\{ECDN>\overline{ECDN_5},EWDN>\overline{EWDN_5}\}}$.

$T_{\{ECDN>\overline{ECDN_5},ECDT<\overline{ECDT_5}\}}$ value decreased, although it increased in Tianjin, Shijiazhuang, Xingtai, and a small part of Baoding [Fig. 9(a)], implying that the risk of occurrence of ECDs increased in most of the BTH region. The $T_{\{ECED>\overline{ECED_5},ECEI<\overline{ECEI_5}\}}$ values generally displayed downward trends [Fig. 9(b)], especially in the areas of Xingtai and Chengde in northern Hebei Province, indicating that the risk of concurrent long-lasting and lower temperature ECEs increased. As for EWDs in wintertime, Fig. 9(c) shows increasing $T_{\{EWDN>\overline{EWDN_5},EWDT>\overline{EWDT_5}\}}$ values in a large part of the BTH region, but significantly decreasing $T_{\{EWDN>\overline{EWDN_5},EWDT>\overline{EWDT_5}\}}$ values in southern and southeastern parts of Guangxi and eastern Guizhou Province. The risk of concurrent long-lasting, higher temperature EWEs in wintertime increased significantly in the colder areas, e.g., Zhangjiakou and Chengde in northern parts of Hebei Province [Fig. 9(d)]. Additionally, the risk of occurrence of EWEs exhibited increasing trends in the urban area and southern parts of Beijing and in eastern areas of Hebei Province. The $T_{\{ECDN>\overline{ECDN_5},EWDN>\overline{EWDN_5}\}}$ values decreased in most areas, implying increased risk of concurrent ECEs and EWEs.

3.4 Spatial–temporal clustering characteristics of wintertime temperature extremes

The spatial–temporal clustering of ETEs in the BTH region during 1978–2018 showed obvious regional differentiation (Fig. 10). The distribution of ECDs and ECEs had strong

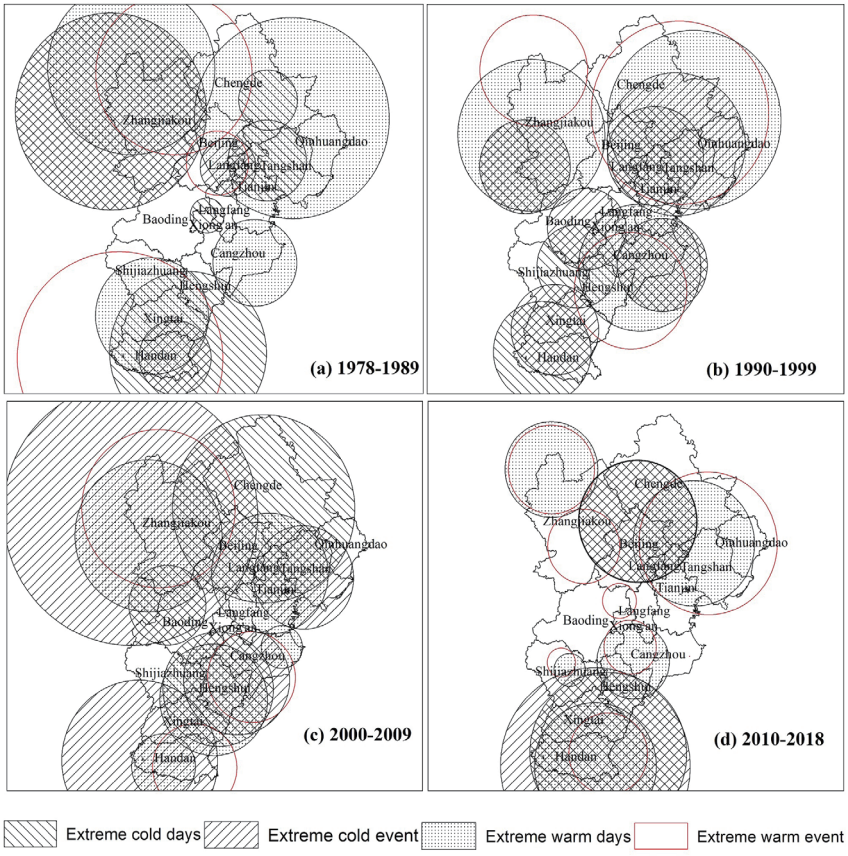

Fig. 10. (Color online) Spatial–temporal clustering of ETEs in the BTH region.

overlap, which means that those regions with more ECDs were also the regions with more ECEs. The spatial overlapping of areas of ECDs and ECEs was distributed mainly in the northern areas of Hebei Province, e.g., Zhangjiakou and Chengde. Similarly, the distribution of EWDs and EWEs also had strong overlap. During 2010–2018, the areas in which EWEs occurred increased significantly, whereas the areas of occurrence of ECEs decreased. The period of 2000–2009 had the greatest spatial–temporal clustering of ETDs and ETEs. For cities located in the central plains, e.g., Tianjin and Baoding, the hazard-formative environment was relatively stable and the spatial–temporal clustering of ETEs was low. There was also less (more) clustering of ETEs in the Beijing Plain area during 1978–1999 (after 2000).

During 1978–2018, clear differences appeared in the migration of the center of gravity of ETEs in the BTH region (Fig. 11). In terms of migration amplitude, the longitudinal variation coefficient was as follows: ECE (0.001) < EWD (0.002) < ECD (0.003) < EWE (0.006), and the latitudinal variation coefficient was as follows: ECE (0.007) < EWD (0.015) < EWE (0.025) < ECD (0.067). The spatial variation of ECEs and EWDs was relatively small, whereas EWEs mainly moved in east–west meridional jumps, and the variation of ECDs was dominated mainly by a north–south latitudinal change. The center of gravity of ECDs migrated counterclockwise, first to the southwest and then to the east. The center of gravity of ECEs moved westward and then northeastward. The center of gravity of EWDs first moved northward and then westward. The position of the center of gravity of EWEs migrated counterclockwise, moving first to the northeast and then to the west.

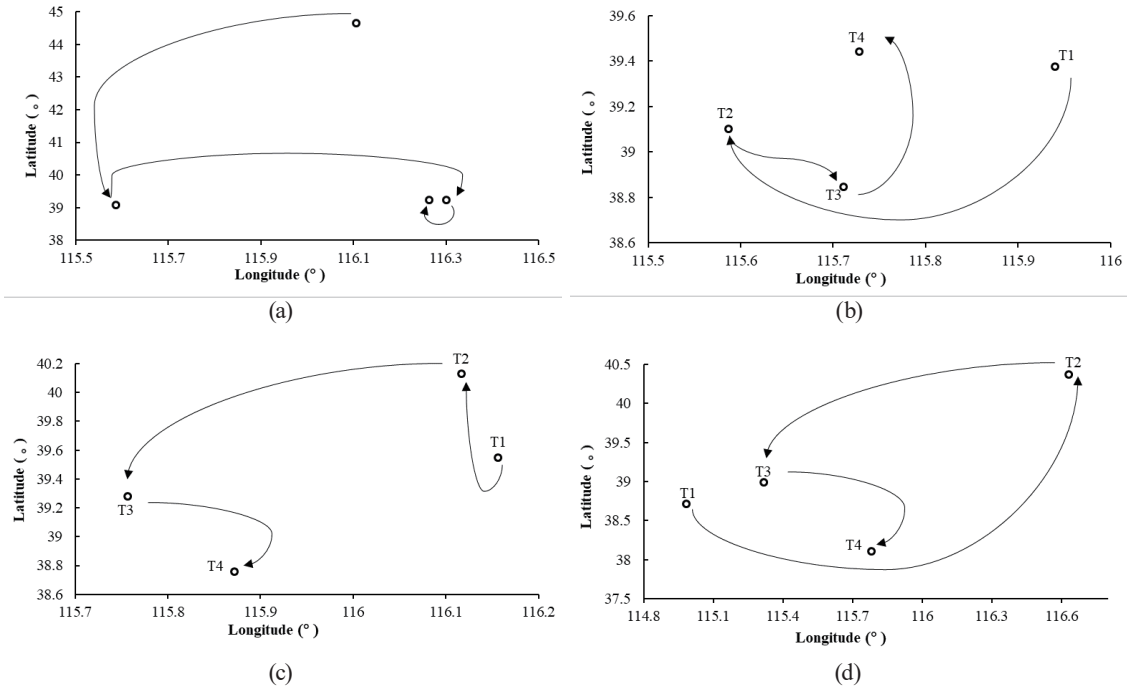

Fig. 11. Migration of center of gravity of ETEs in the BTH region in 1978–2018: T1: 1978–1989, T2: 1990–1999, T3: 2000–2009, and T4: 2010–2018. Gravity center migration of (a) ECDs, (b) ECEs, (c) EWDs, and (d) EWEs.

4. Discussion

Previous studies investigated the features of wintertime ECEs or EWEs across China or certain regions of China.[4,8] However, comprehensive understanding regarding the probability or risk of temperature extremes in winter remains lacking. The minimum absolute temperature can be lower than −30 ℃ in some bitterly cold winters in northern parts of the BTH region, whereas maxima can exceed 20 ℃ in some warm winters in the south of the BTH region. Wintertime ETEs have occurred frequently in the previous several years in the BTH region, causing adverse socioeconomic effects. In this study, multivariate indicators and copulas were used to quantitatively analyze the risks of ETEs and their changing characteristics in wintertime.

We defined eight indexes of wintertime temperature extremes and investigated their changing trends and probabilistic characteristics. Results showed that for ECEs in winter, ECDN at most stations in the BTH region generally showed a significant decreasing trend, whereas the other ECE indexes generally had insignificant changing trends. For winter EWEs, the EWDT at more than 50% of stations showed a significant increasing trend, whereas the other EWE indexes generally showed insignificant changing trends. At the regional scale, ECDN showed an overall trend of significant decreases, EWDN and EWED had trends of significant increases, and trends for all other indexes were insignificant ($p > 0.01$). Nevertheless, the insignificantly changing indexes still implied that winters in the BTH region generally became warmer (the regional averaged daily minimum temperature increased by 0.8 °C per decade over the previous 40 years).

Results suggested that the 5-year return levels for the selected ECE indexes exhibited strong regional characteristics. The $ECDT_5$ increased from −20 °C in the north of the BTH region, to −10 °C in Beijing, and −6 °C in Tianjin and the southern BTH region. The values of $ECED_5$, ECEI5, and ECDT5 generally increased from northern parts toward southern parts of the study area. For the 5-year return levels for the EWE indexes, only $EWDT_5$ exhibited strong regional features, and the difference between the northern BTH region and the southern BTH region reached 20 °C. Spatial variations for the 5-year return levels of the other EWE indexes were marginally significant.

The 5-year return levels generally represent the maximum magnitudes of the indexes at 80% probability of occurrence. The results implied that the severity of potential winter ETEs was relatively high in the northern BTH region, demonstrated by the longer durations of ECEs and EWEs (higher $ECED_5$ and higher $EWED_5$; Fig. 5). Additionally, the changing patterns of the 5-year return levels for the ECE indexes in the two periods studied revealed that the severity of potential ECEs increased during 1999–2018 in the northern BTH region, demonstrated by the increasing trends of $ECDN_5$ and $ECED_5$ [Figs. 6(a) and 6(c)] and the decreasing trends of $ECDT_5$ and $ECEI_5$ [Figs. 6(b) and 6(d)] in the northern BTH region. Furthermore, the increasing trends of the 5-year return levels for the EWE indexes also implied an increasing magnitude of possible EWEs over the previous decades [Figs. 6(e)–(h)].

Based on the results of the joint return periods (Fig. 8) and the corresponding variation characteristics (Fig. 9), it could be inferred that the BTH region may have a relatively high risk of ECEs. The number of extreme cold days have increased, the minimum temperatures have become lower over the previous 20 years, and the probability of ECEs with longer duration and

lower temperatures has increased since 1999. Low $T_{\{EWDN>\overline{EWDN_5},EWDT>\overline{EWDT_5}\}}$ and $T_{\{EWED>\overline{EWED_5},EWEI>\overline{EWEI_5}\}}$ values (Fig. 8) indicated that the central BTH region, e.g., Beijing and Shijiazhuang, is characterized by the high risk of EWEs. However, the significant increasing risk of EWEs occurred in the northern BTH region. The BTH region generally suffers high probability of co-occurrence of ECEs and EWEs (i.e., low $T_{\{ECDN>\overline{ECDN_5},EWDN>\overline{EWDN_5}\}}$; Fig. 8) and increasing risk of concurrent ECEs and EWEs, demonstrated by the decreasing value of $T_{\{ECDN>\overline{ECDN_5},EWDN>\overline{EWDN_5}\}}$ shown in Fig. 9.

The trends of the selected indexes showed that the BTH region has generally become warmer (increasing minimum and maximum temperatures) over the previous years. However, the results also indicated that the risk of ECEs has increased. A reasonable explanation is that extreme events are increasing, which might be a feature associated with global climate change.[25] Furthermore, in this study, we also found that in the cooler north of the BTH region, the magnitude of increasing risk of EWEs was relatively high over the previous 20 years; in the warmer south of the BTH region, the magnitude of increasing risk of ECEs was relatively high. It should be noted that such changes in ETEs might have a substantial impact.

The results of spatial–temporal clustering analysis of ETEs showed that the areas in which EWEs occurred increased significantly in the previous 10 years, and that the period of 2000–2009 was the period with the greatest spatial–temporal clustering of ETEs. Furthermore, by analyzing the migration of the center of gravity of ETEs in different periods, it was found that the center of gravity of ECDs gradually migrated from the northern BTH region to the southern parts. The spatial variation of ECEs was smaller and it occurred mainly in the north of the BTH region. The center of gravity of EWDs and EWEs first moved from the south of the region to the north, and then toward the western coastal area (Tianjin). The results of the migration of the center of gravity of ETEs are also consistent with the previous analysis. There is a lack of analysis on the causes of changes in ETEs in wintertime, such as the impact of climate change or urban expansion; this can be carried out in future work. In addition, the remote sensing data of land surface temperature can also be used for analysis.

5. Conclusions

In this study, we investigated the trends and probabilistic characteristics of wintertime temperature extremes in the BTH region to elucidate the implications regarding hazard risks related to ECEs and EWEs. Eight indexes of wintertime temperature extremes were defined, and their changing trends and probabilistic characteristics were investigated. Results showed that only two indexes changed significantly, whereas the other indexes generally had insignificant changing trends. The findings implied that the BTH region is becoming warmer and suffering increasing ETEs in wintertime. However, the risks and the variation patterns of these extreme events are spatially variable. The northern BTH region has relatively high risk of ECEs and increasing risk of ECEs and EWEs. The central BTH region, e.g., Beijing, is characterized by high risk of EWEs, and the probability of the concurrent occurrence of ECEs and EWEs has increased. The southern BTH region generally has relatively low probability of ECEs and EWEs and increasing risk of ECEs and EWEs. These findings suggest that differences in the

characteristics and spatial distribution of ETEs in winter should be carefully considered when undertaking research on climate change, disaster risk assessment, and city geospatial governance.

Acknowledgments

This research was supported by grant no. 22NLTSY004 from the special joint research project for meteorological capacity improvement of China Meteorological Administration and grant no. B-2022-056 from the China Meteorological Administration for the business support capacity building of meteorological disaster risk service.

References

1 J. A. Screen, C. Deser, and L. Sun: Bull. Am. Meteorol. Soc. **96** (2015) 1489. https://doi.org/10.1175/BAMS-D-14-00185.1
2 J. Cohen, J. A. Screen, J. C. Furtado, M. Barlow, D. Whittleston, D. Coumou, J. Francis, K. Dethloff, D. Entekhabi, and J. Overland: Nat. Geosci. **7** (2014) 627. https://doi.org/10.1038/ngeo2234
3 J. A. Screen: Nat. Clim. Change **4** (2014) 577. https://doi.org/10.1038/nclimate2268
4 Z. Zuo, R. Zhang, Y. Huang, D. Xiao, and D. Guo: Int. J. Climatol. **35** (2015) 3568. https://doi.org/10.1002/joc.4229
5 X. Zhang and H. Hu: Atmosphere **9** (2018) 263. https://doi.org/10.3390/atmos9070263
6 T.-W. Park, J. G. Hong, and D.-S. R. Park: Int. J. Climatol. **40** (2020) 2639. https://doi.org/10.1002/joc.6356
7 J. Zheng, L. Ding, Z. Hao, and Q. Ge: Boreas **41** (2015) 1. https://doi.org/10.1111/j.1502-3885.2011.00225.x
8 W. Sun, X. Mu, X. Song, D. Wu, A. Cheng, and B. Qiu: Atmos. Res. **168** (2016) 33. https:// doi.org/10.1016/j.atmosres.2015.09.001
9 H. Wang, Y. Chen, Z. Chen, and W. Li: Nat. Hazards **65** (2013) 1913. https://doi.org/10.1007/s11069-012-0454-4
10 M. Honda, J. Inoue, and S. Yamane: Geophys. Res. Lett. **36** (2009) 262. https://doi.org/10.1029/2008GL037079
11 Q. You, G. Ren, K. Fraedrich, S. Kang, Y. Ren, and P. Wang: Int. J. Climatol. **33** (2013) 1444. https://doi.org/https://doi.org/10.1002/joc.3525
12 H. Deng, Y. Chen, X. Shi, W. Li, H. Wang, S. Zhang, and G. Fang: Atmos. Res. **138** (2014) 346. https://doi.org/https://doi.org/10.1016/j.atmosres.2013.12.001
13 S. J. Brown, J. Caesar, and C. A. T. Ferro: J. Geophys. Res.: Atmos. **113** (2008). https://doi.org/10.1029/2006JD008091
14 M. Sklar: Publ. Inst. Stat. Univ. Paris **8** (1959) 229
15 P. K. Trivedi and D. M. Zimmer: Found. Trends® Econom. **1** (2007) 1. https://doi.org/10.1561/0800000005
16 M. Liu, X. Xu, A. Y. Sun, K. Wang, W. Liu, and X. Zhang: Environ. Res. Lett. **9** (2014) 064002. https://doi.org/10.1088/1748-9326/9/6/064002
17 U. F. A. Rauf and P. Zeephongsekul: Theor. Appl. Climatol. **115** (2014) 153. https://doi.org/10.1007/s00704-013-0877-1
18 S. Vandenberghe, N. E. C. Verhoest, C. Onof, and B. De Baets: Water Resour. Res. **47** (2011) 197. https://doi.org/10.1029/2009WR008388
19 V. P. Singh and L. Zhang: J. Hydrol. Eng. **11** (2006) 150. https://doi.org/10.1061/(ASCE)1084-0699(2006)11:2(150)
20 D. D. Zhang, D. H. Yan, F. Lu, Y. C. Wang, and J. Feng: Nat. Hazards **75** (2015) 2199. https://doi.org/10.1007/s11069-014-1419-6
21 C. J. Willmott, S. G. Ackleson, R. E. Davis, J. J. Feddema, K. M. Klink, D. R. Legates, J. O'Donnell, and C. M. Rowe: J. Geophys. Res.: Oceans **90** (1985) 8995. https://doi.org/10.1016/0198-0254(86)91285-9
22 S. Kisilevich, F. Mansmann, M. Nanni, and S. Rinzivillo: Spatio-Temporal Clustering: In Data Mining and Knowledge Discovery Handbook (Springer US, Boston, MA, 2010) p. 855. https://doi.org/10.1007/978-0-387-09823-4_44
23 M. Kulldorff: Commun. Stat.- Theory Methods **26** (1997) 1481. https://doi.org/10.1080/03610929708831995
24 M. Kulldorff, R. Heffernan, J. Hartman, R. Assunção, and F. Mostashari: PLoS Med. **2** (2005) e59. https://doi.org/10.1371/journal.pmed.0020059
25 Y. Sun, X. Zhang, F. W. Zwiers, L. Song, H. Wan, T. Hu, H. Yin, and G. Ren: Nat. Clim. Change **4** (2014) 1082. https://doi.org/10.1038/nclimate2410